

Chemical Science

Accepted Manuscript

This article can be cited before page numbers have been issued, to do this please use: J. Goodall, M. A. Sajjad, S. K. Furfari, T. S. Hatcher, A. S. Weller, S. A. Macgregor, J. M. Lynam, M. R. Warren, S. J. Page, G. J. Tizzard and K. M. Altus, *Chem. Sci.*, 2026, DOI: 10.1039/D6SC02133F.



This is an Accepted Manuscript, which has been through the Royal Society of Chemistry peer review process and has been accepted for publication.

Accepted Manuscripts are published online shortly after acceptance, before technical editing, formatting and proof reading. Using this free service, authors can make their results available to the community, in citable form, before we publish the edited article. We will replace this Accepted Manuscript with the edited and formatted Advance Article as soon as it is available.

You can find more information about Accepted Manuscripts in the [Information for Authors](#).

Please note that technical editing may introduce minor changes to the text and/or graphics, which may alter content. The journal's standard [Terms & Conditions](#) and the [Ethical guidelines](#) still apply. In no event shall the Royal Society of Chemistry be held responsible for any errors or omissions in this Accepted Manuscript or any consequences arising from the use of any information it contains.

ARTICLE

The Characterisation and Reactivity of a Rh^{III} η¹-σ-Alkane Complex and the Role of a Structurally Responsive Phosphine Ligand in Solid-State Molecular Organometallic Chemistry

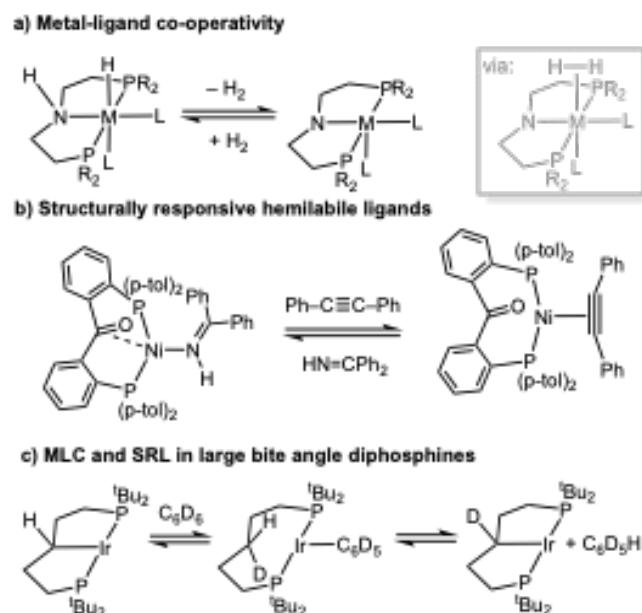
Joe C. Goodall,^{a*} M. Arif Sajjad,^b Samantha K. Furfari,^a Kristof M. Altus,^a Theo S. C. Hatcher,^b Graham J. Tizzard,^c Samuel J. Page,^d Mark R. Warren,^e Jason M. Lynam,^{a*} Stuart A. Macgregor,^{b*} and Andrew S. Weller^{a*}

A combined experimental and computational study on the single-crystal to single-crystal addition of H₂ to [Rh(κ²-dtbpb)(NBD)][BAR^f₄] [dtbpb = ^tBu₂P(CH₂)₄P^tBu₂, NBD = norbornadiene, Ar^f = 3,5-C₆H₃(CF₃)₂] to give the Rh(III) η¹-σ-alkane complex [Rh(dtbbpb')(H)(η¹-C₇H₁₂)] [BAR^f₄] (dtbbpb' = κ³-PCP-^tBu₂PCH₂CHCH₂CH₂P^tBu₂) is reported, in which the supporting phosphine ligand has also undergone C–H activation of one of the methylene groups in the chelate backbone to form a *trans*-spanning κ³-pincer-type ligand. Characterisation by variable temperature single-crystal X-ray diffraction, solid-state NMR spectroscopy, periodic DFT and IGHM/QTAIM calculations support this assignment, and also that the norbornane (NBA) alkane ligand can access low energy conformational isomers in the solid-state. Dissolving in CD₂Cl₂ displaces the alkane and the corresponding solvent adduct is formed, [Rh(dtbbpb')(H)(κ¹-ClCD₂Cl)] [BAR^f₄]. DFT calculations, supported by experiment, indicate the C–H activation of the backbone occurs after full hydrogenation of the NBD to NBA, and not at a norbornene intermediate. Addition of propene to the crystalline σ-alkane complex displaces the NBA, and the phosphine ligand responds by reforming the κ²-motif, consistent with C–H activation being thermodynamically favoured when *trans* to a weakly coordinating σ-alkane. These reversible bond activations of the chelating ligand in response to changes in the co-ligands demonstrate that significant structural reorganisation is possible in the crystalline environment.

Introduction

The non-innocent role ligands can play in organometallic reaction mechanisms has become an important design principle that is used for the delivery of efficient, lower energy, and selective homogeneous catalytic processes. Central to such active ligand participation are the concepts of metal-ligand cooperativity (MLC) and structurally responsive ligands (SRL). MLC^{1–3} involves the ligand taking a role in bond activation processes, that often involve the shuttling of protons/hydrides in a catalytic manifold between the metal centre and ligand, e.g. in (de)hydrogenation reactions,^{4, 5} Scheme 1a. SRLs show dynamic structural behavior;^{6–9} such as hemilability – in which a ligand can adapt to changes at the metal centre by offering a variety of accessible coordination modes, e.g. Scheme 1b.¹⁰ Large bite-angle κ²-chelating diphosphines, e.g. R₂P(CH₂)₅PR₂, have been shown to capture aspects of both MLC and SRL reactivity, undergoing (reversible) backbone C–H activation at the metal centre to form κ³-PCP-type carbometallated pincer

ligands,^{11–13} that have the potential to facilitate bond activation processes such as H/D exchange, Scheme 1c.^{14–16}



Scheme 1 a) Schematic metal-ligand co-operativity (R = alkyl, aryl).^{2,4} b) Example of a hemilabile ligand.¹⁰ c) Suggested mechanism for H/D exchange at a 14e intermediate using large bite-angle phosphines.¹⁵

^a Department of Chemistry, University of York, York, YO10 5DD, UK

^b EaStCHEM School of Chemistry, University of St Andrews, North Haugh, St Andrews, KY16 9ST, UK

^c UK National Crystallography Service, School of Chemistry and Chemical Engineering, University of Southampton, Southampton, SO17 1BJ, UK

^d Department of Chemistry, University of Durham, Durham, DH1 3LE, UK

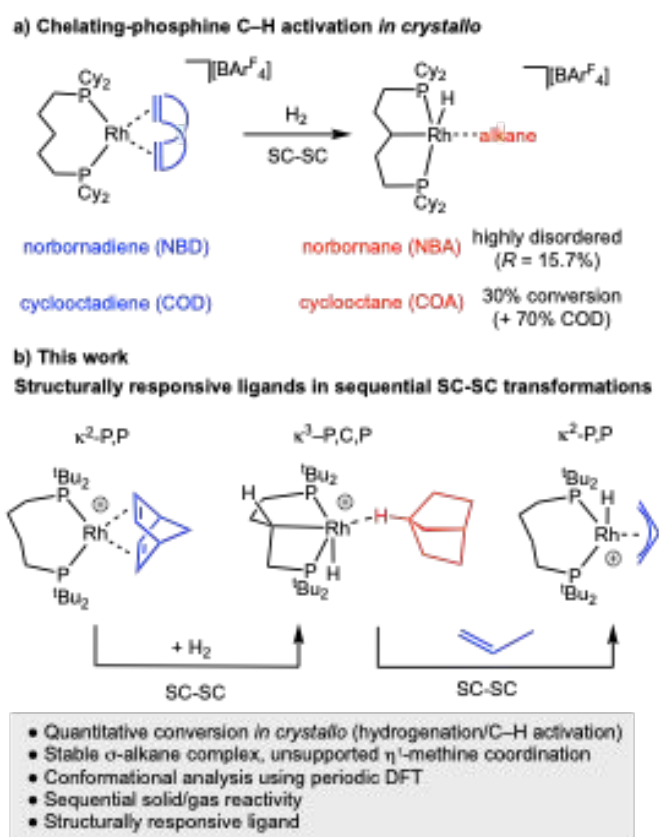
^e Diamond Light Source Ltd, Didcot OX110DE, UK.

Supplementary Information available: See DOI: 10.1039/x0xx00000x



We have been developing the concept of solid-state molecular organometallic chemistry (SMOM¹⁷), where solid/gas reactivity *in crystallo*^{18, 19} allows for the isolation and detailed characterisation of σ -alkane complexes by single-crystal to single-crystal (SC-SC) transformations.^{20, 21} While σ -alkane complexes are generally unstable in solution, being characterised *in situ* at low temperature using photolysis^{22, 23} or protonation^{24, 25} routes; by optimal design of metal complex, solvent and reaction conditions, σ -alkane complexes can be recrystallised from solution.^{26–30} Using this SMOM approach we have also shown that a wide variety of fundamental organometallic mechanistic steps are supported in crystalline molecular reactivity. Examples include: (reversible) C–H activation of a bound alkane ligand,^{31–33} migratory insertion,^{34, 35} ligand substitution,^{36–38} C–N bond formation,³⁹ and isotope effects.^{32, 33, 40} We have also reported that $[\text{Rh}(\text{Cy}_2\text{P}(\text{CH}_2)_5\text{PCy}_2)(\text{alkene})][\text{BAR}^f_4]$ (alkene = norbornadiene, NBD, or 1,5-cyclooctadiene, COD; $\text{Ar}^f = 3,5\text{-(CF}_3)_2\text{C}_6\text{H}_3$), can undergo backbone C–H activation on addition of H_2 to give a carbometallated κ^3 -PCP ligand complex with a σ -alkane ligand, Scheme 2a.⁴¹ However, the norbornane (NBA) is highly disordered precluding detailed characterisation, while the cyclooctane (COA) σ -alkane complex is only generated in ~30% maximum conversion from the COD precursor *in crystallo* before onward decomposition occurs.

In this contribution we show that by using the wide bite-angle, κ^2 -PP phosphine ligand, $^t\text{Bu}_2\text{P}(\text{CH}_2)_4\text{P}^t\text{Bu}_2$, the quantitative conversion to a stable η^1 - σ -alkane complex of



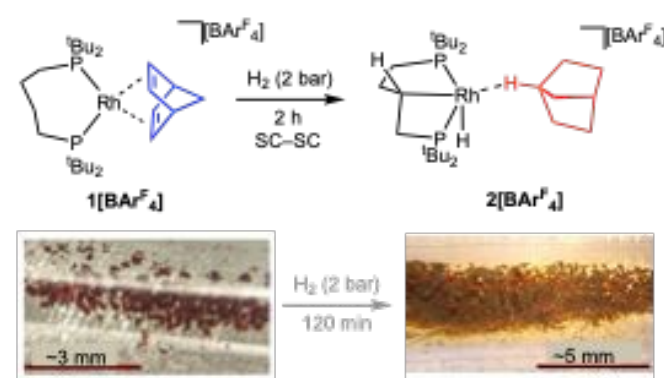
Scheme 2 a) Prior SMOM work showing C–H activation of a P,P-ligand. b) This work. $[\text{BAR}^f_4]^-$ anions are not shown.

NBA is achieved on hydrogenation of the NBD precursor. A rare example of a carbometallated κ^3 -PCP ligand with a C–C backbone is also formed through C–H activation of the phosphine backbone, Scheme 2b. We show that this is a structurally responsive ligand *in crystallo*, as addition of propene reforms the κ^2 -PP ligand; and provide evidence for the likely order of events in the mechanism of C–H activation. These reversible bond activations of the chelating ligand in response to changes in the co-ligands (NBD/NBA/propene) demonstrate that the molecular single-crystal environment can support significant structural reorganisation that is a characteristic of MLC and SRLs, so well-documented in the solution phase.

Results and Discussion

Synthesis and characterisation of precursor $[\text{Rh}(\text{dtbpb})(\text{NBD})][\text{BAR}^f_4]$, $1[\text{BAR}^f_4]$. The precursor complex, $[\text{Rh}(\text{dtbpb})(\text{NBD})][\text{BAR}^f_4]$ $1[\text{BAR}^f_4]$ [dtbpb = $^t\text{Bu}_2\text{P}(\text{CH}_2)_4\text{P}^t\text{Bu}_2$] was prepared by addition of dtbpb to $[\text{Rh}(\text{NBD})_2][\text{BAR}^f_4]$ in CH_2Cl_2 solution. Recrystallisation from CH_2Cl_2 /hexane produced analytically pure deep-red crystals of $1[\text{BAR}^f_4]$ in 88% yield (ESI). The solid-state structure of $1[\text{BAR}^f_4]$, as determined by single-crystal X-ray diffraction ($P2_1/n$, $R_1 = 3.15\%$), reveals a pseudo square-planar cation, Figure 1a. The cation is located within an approximate octahedral cage of $[\text{BAR}^f_4]^-$ anions (Figures 1b, c) as we have noted for other $[\text{Rh}(\text{L}_2)(\text{NBD})][\text{BAR}^f_4]$ SMOM systems that undergo solid/gas reactivity.^{20, 31, 32, 34, 41} Some NBD alkene protons show close non-covalent $\text{C–H}\cdots\text{F}$ contacts with the CF_3 groups of proximate anions, e.g. $\text{H}1\cdots\text{F}22$ 2.6148(15) Å; $\text{H}2\cdots\text{F}21$ 2.7007(15); $\text{H}3\cdots\text{F}13$, 3.0951(17) Å. There is no crystallographically imposed symmetry in the cation, and this is reflected in the $^{31}\text{P}\{^1\text{H}\}$ SSNMR spectrum in which two environments are observed [δ 42.8 and 25.0; $J(\text{RhP}) = 148$ Hz], similar to those reported for $[\text{Rh}(^t\text{Bu}_2\text{P}(\text{CH}_2)_3\text{P}^t\text{Bu}_2)(\text{NBD})][\text{BAR}^f_4]$.⁴³ In the $^{13}\text{C}\{^1\text{H}\}$ SSNMR spectrum signals between δ 77.1 and 48.2 are assigned to the alkene groups of the NBD ligand. C_{2v} symmetry is observed in the solution NMR spectra (ESI).

Synthesis of $[\text{Rh}(\text{dtbpb})(\text{H})(\text{NBA})][\text{BAR}^f_4]$, $2[\text{BAR}^f_4]$: Ligand non-innocence. Addition of H_2 (2 bar, 2 h) to single-crystalline $1[\text{BAR}^f_4]$ results in a SC-SC transformation and a colour change from deep red to sandy yellow complex, Scheme 3, in which



Scheme 3 Synthesis of complex $2[\text{BAR}^f_4]$. Inset shows optical microscopy of the crystals pre- and post-addition of H_2 .



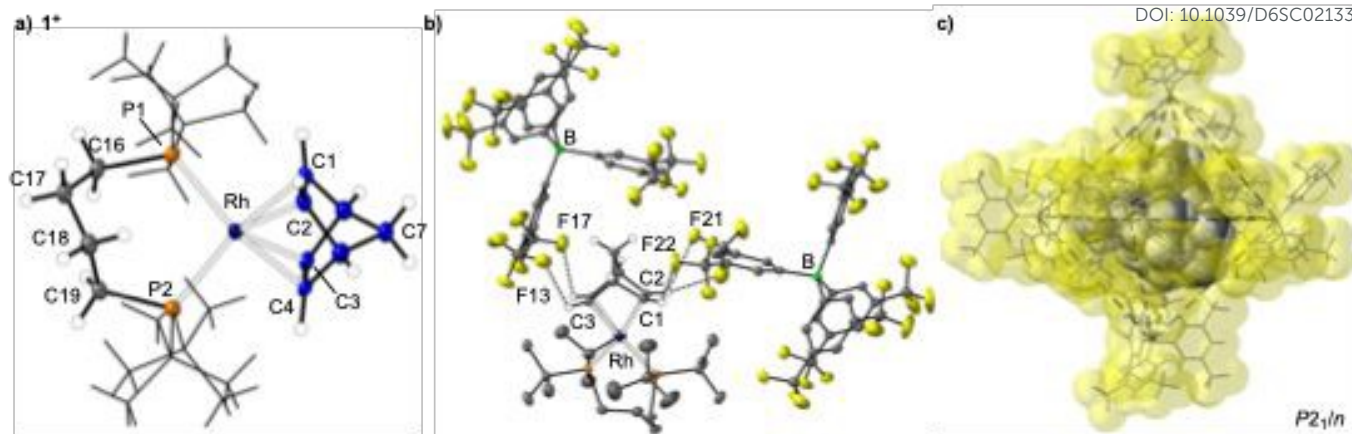


Figure 1 Solid-state structure of **1[BARF₄]** a) Structure of the cation, **1⁺**. Displacement ellipsoids are shown at the 50% probability level, selected H-atoms shown, ^tBu groups shown in stick form. Selected bond lengths (Å) and angles (°). Rh–P1, 2.4412(5); Rh–P2, 2.4252(5); C1–C2, 1.390(3); C3–C4, 1.393(3); Rh⋯C18, 3.8103(19); P1–Rh–P2, 102.110(17). b) Extended asymmetric unit showing the relationship between two proximal [BARF₄][−] anions and the metal centre. F⋯H contacts less than 3.1 Å shown (range 3.095 – 2.614 Å). c) Arrangement of [BARF₄][−] anions around the **1⁺** cation. Cation atoms and anion surfaces shown at van der Waals radii

the supporting phosphine ligand has also undergone C–H activation (carbometallation) of one of the methylene groups in the chelate backbone to give [Rh(dtbpb')](H)(η¹-C₇H₁₂)[BARF₄]**2[BARF₄]** (dtbpb' = κ³-PCP-^tBu₂PCH₂CHCH₂CH₂P^tBu₂).

On addition of H₂, the NBD ligand in **1[BARF₄]** is hydrogenated to norbornane which remains coordinated to the Rh centre through a bridgehead methine C–H group, forming an η¹-σ(C–H)-NBA complex,²⁵ Rh1⋯C5 = 3.009(5) Å. While in the initial structural refinements the NBA ligand was unrestrained, its associated displacement ellipsoids were large and some C–C bond lengths were long (~1.7 Å), indicating unresolved disorder. These separate disordered components could not be satisfactorily modelled. For this reason, the C–C distances in the NBA were lightly restrained to lie within a range of 1.385 – 1.656 Å. Nevertheless, the conversion from NBD to NBA on hydrogenation is unambiguous based on the change in

coordination mode from an η²η² alkene ligand in **1[BARF₄]** to a η¹-σ-alkane ligand in **2[BARF₄]**. While a η¹-methine Rh⋯H–C interaction has been noted in a structurally characterised σ-alkane methylpentane⁴⁴ complex, the Rh⋯H–C interaction in that case is also supported by being part of a chelating alkane ligand. An *unsupported* η¹-Rh⋯H–C interaction has been observed in a cyclooctane complex (Figure 2a), but here it arises from a methylene group.⁴¹ The unsupported η¹-binding methine mode of the alkane in **2[BARF₄]** is new for a structurally characterised alkane σ-complex interactions in the solid-state^{42, 45} (methyl, methylene, methine;^{26, 27, 44} η²η²^{20, 40} through to η¹^{41, 44}), mirroring those measured in solution using low temperature *in situ* NMR methods.^{22, 25, 46}

Hydrogenation of NBD is accompanied by one methylene group (C18) of the chelating phosphine undergoing C–H

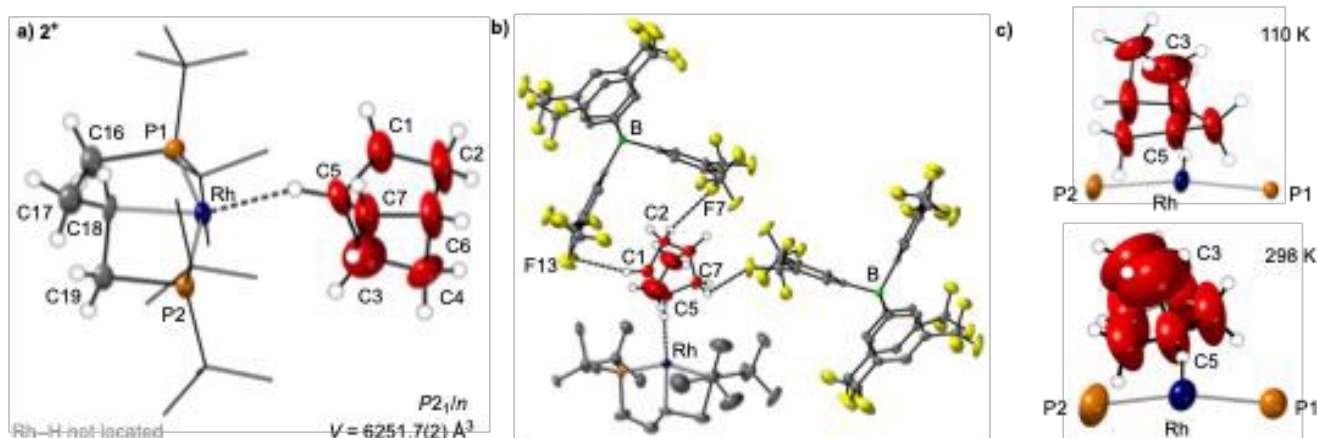


Figure 2 Solid-state structure of **2[BARF₄]** a) Structure of the cation, **2⁺**. Only one disordered component (C18/C18A disorder) shown. See main text and ESI. Displacement ellipsoids are shown at the 30% probability level, selected H-atoms shown, ^tBu groups shown in stick form. The Rh–hydride was not located and is not shown. Selected bond lengths (Å) and angles (°). Rh–P1, 2.2968(9); Rh–P2, 2.3284(11); C1–C2, 1.516(7); C3–C4, 1.502(10)[°]; Rh1⋯C5, 3.009(5); Rh1–C18, 2.076(11); P1–Rh–P2, 154.86(4); C18–Rh–C5, 164.5(5) b) Extended asymmetric unit showing the relationship between two proximal [BARF₄][−] anions and the metal centre. F⋯H contacts less than 3.1 Å shown (range 2.880 – 2.696 Å). c) Comparison of displacement ellipsoids (30% probability) of the structure of **2[BARF₄]** collected at 110K and 298 K. Only Rh, P atoms and NBA group shown. Selected distances and angles (see Figure 2a) Rh–C18: 110K, 2.076(11); 298 K, 2.111(15) Å; 110K, P1–Rh–P2, 154.86(4); 298 K, 155.27(9)[°]. [° NBA C–C distances lightly restrained to within a range of 1.385 – 1.656 Å. See ESI.]



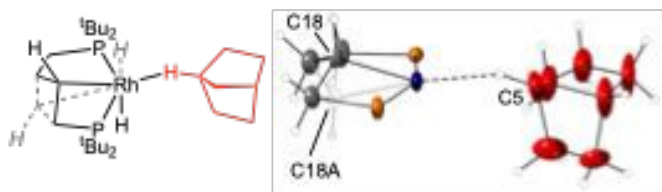


Figure 3. Disorder model for the C4-backbone of $2[\text{BArF}_4]$ at C18/C18A.

activation to form an unsymmetrical, *trans* spanning κ^3 -PCP pincer ligand: Rh–C18, 2.076(11) Å, P1–Rh–P2 = 154.86(4)°. The alkane ligand sits *trans* to this new bond [C18–Rh–C5 = 164.5(5)°]. This Rh–C bond in $2[\text{BArF}_4]$ is disordered over two positions, with C18/C18A sitting above or below the RhP₂ plane, modelled as a 60:40 split, Figure 3. The corresponding Rh–hydride and C18–H were not located. Their presence was confirmed by solution studies of the corresponding CH₂Cl₂ adduct, $3[\text{BArF}_4]$, that shows the hydride sitting *anti* disposed relative to the C–H bond, *vide infra*. There are no close interactions (Rh...C < 3.5 Å) between the ^tBu groups and the vacant site *trans* to the hydride.

C–H activation of a C₅ phosphine backbone is relatively common in solution-based organometallics,^{11–13} but only one example involving a C₄ phosphine is known,⁴⁷ although related complexes have been reported.⁴⁸ Intramolecular ligand activation in SC–SC *in crystallo* transformations have been reported, for example C–H^{32, 33, 49, 50} and C–C activation.^{51, 52}

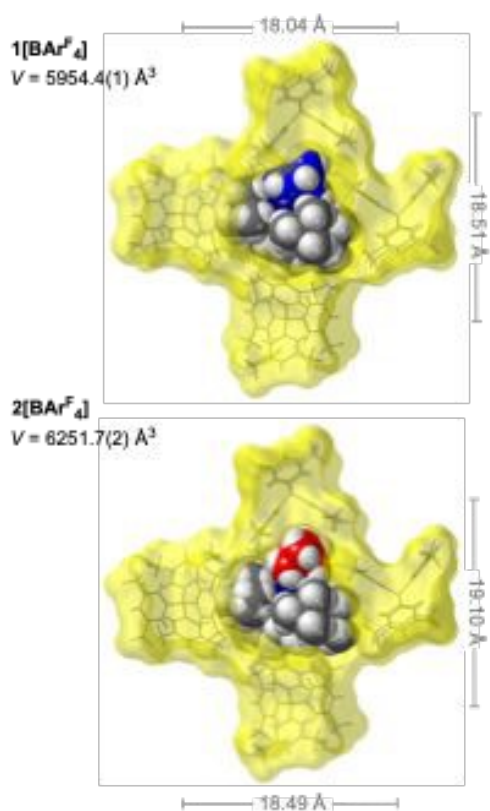


Figure 4. Comparison of anion cage metrics between $1[\text{BArF}_4]$, and $2[\text{BArF}_4]$. Front $[\text{BArF}_4]$ anion removed for clarity. Van Der Waals radii. Distances shown are B...B cross-cage distances.

While the structural change on alkene hydrogenation and C–H activation of the phosphine is significant, the overall arrangement of $[\text{BArF}_4]^-$ anions remain unchanged from $1[\text{BArF}_4]$, with the similar C–H...F hydrogen bonding observed from the proximal anions, Figure 2b. The structural plasticity of the $[\text{BArF}_4]^-$ anions, likely facilitated by the –CF₃ groups,^{37, 53–55} allows for the arrangement of anions to breathe to accommodate the changes at the cation, with cross-cage B...B distances increasing slightly, alongside a 5% change in unit cell volume, Figure 4.

The formation of $2[\text{BArF}_4]$ is supported by the analysis of bulk materials (~50mg sample size) using ³¹P{¹H} and ¹³C{¹H} SSNMR spectroscopy at 298K, Figure 5 (see ESI for the ¹³C{¹H} SSNMR spectrum). On hydrogenation the chemical shifts of the two ³¹P environments become more disperse, δ 100.6 and δ –8.7, consistent with the formation of 5 and 4 membered cyclometallated rings.⁴⁷ The lower field signal at δ 100.6 is observed as a doublet of doublets [*J*(PP) 280 Hz, *J*(RhP) 115 Hz], while the higher field signal is observed as an apparent triplet [*J*(PP) ~300 Hz] that is significantly broader [fwhm = 800 Hz]. These data are consistent with the generation of a Rh(III) centre with *trans*-spanning phosphines.⁵⁶ The apparent triplet is interpreted as being formed of two overlapped doublets, in which the ¹⁰³Rh–³¹P coupling is not resolved (i.e. it is small), assigned to each C18/C18A disordered component in $2[\text{BArF}_4]$. These are suggested to be coincident for the two components in higher chemical shift signal. The ¹³C{¹H} SSNMR spectrum

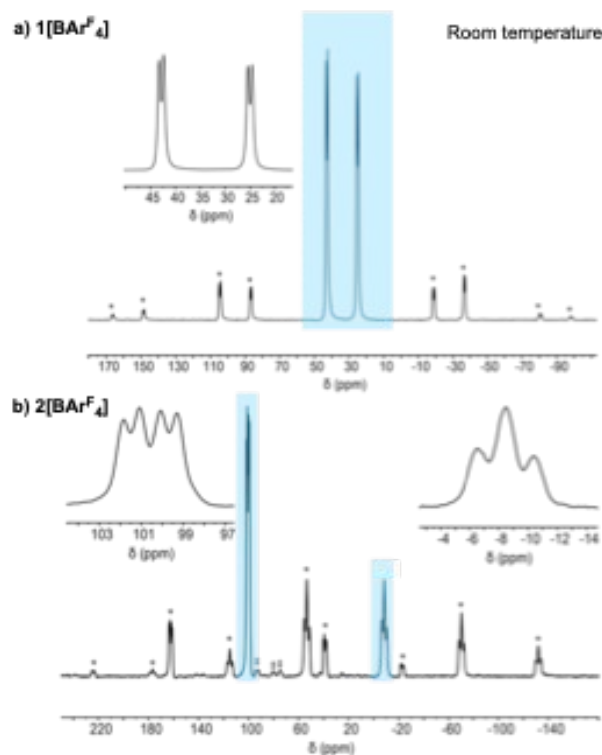


Figure 5. ³¹P{¹H} SSNMR spectra (162 MHz, 10 kHz spin rate, room temperature) of a) $1[\text{BArF}_4]$, and b) $2[\text{BArF}_4]$. * Spinning-side bands. † Unidentified product. Light blue highlighted areas indicate the isotopic chemical shifts, insets show these in more detail.



shows an absence of signals in the alkene region (δ 110 – 50). When dissolved in CD_2Cl_2 solution only one set of signals are observed (vide infra).

The disorder of the bound NBA alkane ligand observed in **2**[BAR^{F_4}] was probed using variable temperature single-crystal X-ray diffraction studies (215 K and 298 K). These higher temperatures increase the size of the displacement ellipsoids, Figure 2c, and the errors on the unrestrained C–C bond lengths and angles in the NBA, while C18/C18A of the phosphine backbone become undistinguishable. These data suggest there is a dynamic process occurring at the coordinated alkane, that results in a superposition of a variety of different conformers for the alkane ligand, that becomes more apparent on warming.

To probe this further, periodic-DFT calculations were employed in conjunction with conformational searching with CREST⁵⁷ to model different η^1 -alkane binding modes in **2**[BAR^{F_4}] (ESI). These confirmed the experimental structure bound through a bridgehead C–H bond (i.e. C5) to be lowest in energy while also locating alternative η^1 -isomers (Figure 6a) bound through an *endo*-C–H bond (at +1.8 kcal/mol), an *exo*-C–H bond (at +2.8 kcal/mol), and a methylene bridge C–H bond (at +2.1 kcal/mol). Additional rotamers of the experimental structure were also located at +0.4 and +6.7 kcal/mol. Thus, a series of low energy alternative structures are readily accessible that, assuming low barriers for interconversion, are consistent with dynamic disorder of the NBA ligand at the Rh centre, as signalled by the large displacement ellipsoids evident in the experimentally-determined 298 K structure (Figure 2c).

The nature of the $\text{Rh}\cdots\text{NBA}$ interaction was assessed via QTAIM, NBO and Independent Gradient Model (Hirshfeld partitioning, IGMH) calculations. These used the experimental structure of **2**[BAR^{F_4}] with the H and F positions refined through a periodic-DFT optimisation. With this model $\text{Rh}\cdots\text{H5}$ and $\text{H5}\cdots\text{C5}$ distances of 1.99 Å and 1.12 Å are computed and a $\text{Rh}\cdots\text{H5}\cdots\text{C5}$ angle of 150°. The QTAIM molecular graph (Figure 6b) exhibits a $\text{Rh}\cdots\text{H5}\cdots\text{C5}$ bond path with a bond critical point (BCP) electron density, $\rho(r)$, of 0.042 au, consistent with previous examples of $\eta^1\text{-C-H}\cdots\text{Rh}$ binding while somewhat lower than $\eta^2\text{-C-H}\cdots\text{Rh}$ interactions.⁴⁴ The $\text{C5}\cdots\text{H5}$ BCP ($\rho(r) = 0.252$ au) indicates a weakening due to the σ -interaction with Rh; in comparison $\rho(r) = 0.277$ au at the BCP of the unperturbed $\text{C6}\cdots\text{H6}$ bridgehead bond.

The IGMH plot (Figure 6c) highlights the $\text{H5}\cdots\text{Rh}$ interaction as the strongest atom-atom interaction between the NBA and Rh fragments, with the localised blue disk characteristic of a $\eta^1\text{-C-H}\cdots\text{Rh}$ interaction. Green isosurfaces between the NBA ligand and ^tBu substituents indicate additional van der Waals interactions²⁹ aligning with weak $\text{C-H}^{\text{NBA}}\cdots\text{H-C}^{\text{tBu}}$ bond paths in the QTAIM study ($\rho(r) = 0.003\text{--}0.009$ au; omitted from Figure 6b for clarity; see Figure S28). A 2nd order perturbation analysis within the NBO framework (Figure 6d) indicates $\sigma_{\text{C5-H5}} \rightarrow \sigma_{\text{Rh-C18}}^*$ donation is the strongest individual interaction at 12.3 kcal/mol. $\sigma_{\text{Rh-C18}} \rightarrow \sigma_{\text{C5-H5}}^*$ contributes most to back-donation (6.6 kcal/mol), and once contributions from the $\sigma_{\text{Rh-hydride}}$ and $\sigma_{\text{Rh-P2}}$ orbitals are included the total back-donation is similar in magnitude ($\Sigma = 10.7$ kcal/mol) to $\sigma_{\text{C5-H5}} \rightarrow \text{Rh}$ σ -donation. This is again consistent with previous

$\eta^1\text{-C-H}\cdots\text{Rh}$ motifs and contrasts with $\eta^2\text{-C-H}\cdots\text{Rh}$ interactions where $\text{C-H} \rightarrow \text{Rh}$ σ -donation usually dominates.

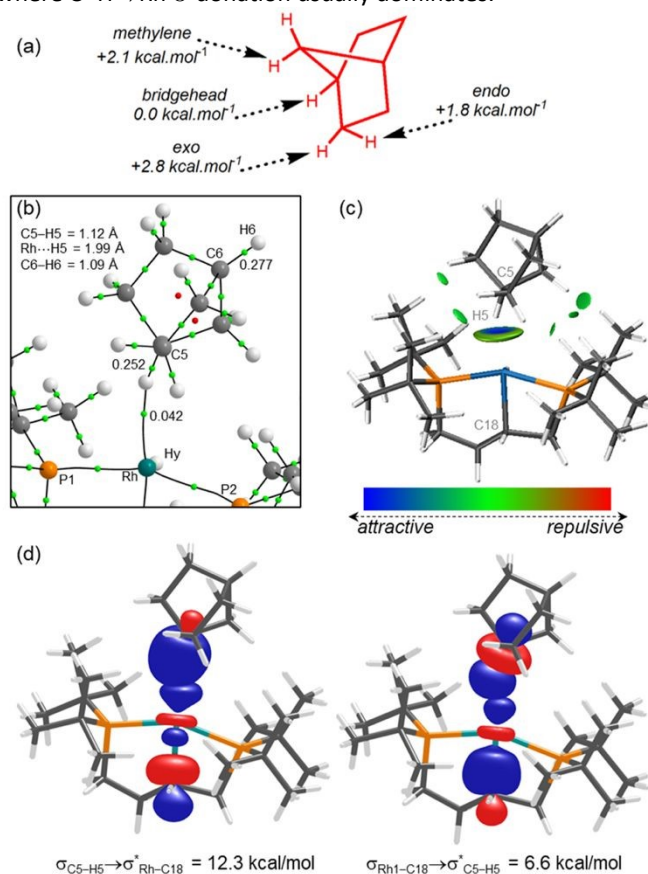
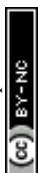


Figure 6 a) Relative energies of $\text{Rh}\cdots\text{H-C}$ interactions with the NBA ligand in **2**[BAR^{F_4}]. b) Detail of the QTAIM molecular graph of the cation of **2**[BAR^{F_4}]. c) IGMH plot for the **2**⁺ cation (sign(λ_2) ρ -coloured isosurfaces with $\delta G^{\text{inter}} = 0.001$ au). d) Key donor-acceptor interactions for the $\text{Rh}\cdots\text{NBA}$ interaction as quantified via 2nd order perturbation NBO analyses. Back-donation from $\sigma_{\text{Rh-Hy}}$ and $\sigma_{\text{Rh-P2}}$ contribute 2.4 kcal/mol and 1.7 kcal/mol respectively (see ESI for orbital plots).

Synthesis of $[\text{Rh}(\text{dtbpb}')(\text{H})(\kappa^1\text{-ClCD}_2\text{Cl})][\text{BAR}^{\text{F}_4}]$, **3[BAR^{F_4}].** Vacuum transfer of CD_2Cl_2 onto single crystals of **2**[BAR^{F_4}], resulted in the quantitative formation of a complex in which NBA is no longer coordinated to the metal centre. Recrystallisation from CD_2Cl_2 /heptane at 243 K afforded single crystals suitable for single-crystal X-ray diffraction, that allowed for the identification of the complex as $[\text{Rh}(\text{dtbpb}')(\text{H})(\kappa^1\text{-ClCD}_2\text{Cl})][\text{BAR}^{\text{F}_4}]$, **3**[BAR^{F_4}], Figure 7. The resulting solid-state structure is described first, followed by solution NMR spectroscopic data.

Complex **3**[BAR^{F_4}] crystallised with two crystallographically independent, but structurally very similar, cations in the unit cell. One of these was well defined, Figure 7b, and the other refined best using a three-part disorder model for bound CD_2Cl_2 . Only the bond metrics for the ordered component are discussed. These show a κ^1 -bound CD_2Cl_2 [$\text{Rh1}\cdots\text{Cl1}$, 2.5692(10) Å], that sits *trans* to the carbometallated phosphine backbone [$\text{Rh1}\cdots\text{C18}$, 2.044(4) Å]. The phosphine ligand remains *trans* spanning [$\text{P1}\cdots\text{Rh1}\cdots\text{P2}$ = 154.50(4)°]. The $\text{Rh1}\cdots\text{H}$ and $\text{C18}\cdots\text{H}$ protons were located in the difference map, and sit *anti* to one another. The structure of **3**[BAR^{F_4}] is similar to that reported for



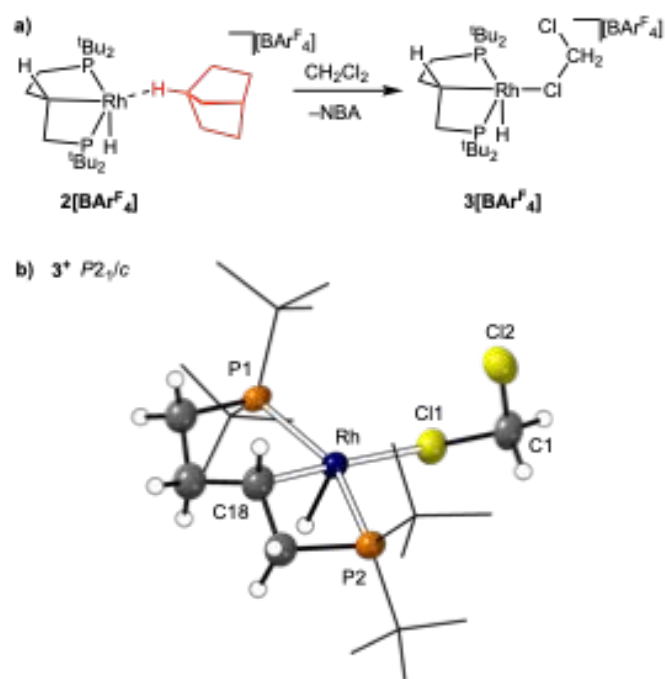


Figure 7 a) Synthesis of $3[\text{BARF}_4]$ b) Solid-state structure of one of the crystallographically-independent cations of 3^+ . Displacement ellipsoids are shown that the 50% probability level, selected H-atoms shown, ^tBu groups shown in stick form. Selected bond distance (Å) and angles ($^\circ$): Rh1–P1, 2.3032(9); Rh1–P2, 2.3366(8); Rh1–C18, 2.044(4); Rh1–Cl1, 2.5692(10); P1–Rh1–P2, 154.50(4); C18–Rh1–Cl1, 178.26(13).

the analogue with the $\text{Cy}_2\text{P}(\text{CH}_2)_5\text{PCy}_2$ ligand;⁴¹ while CH_2Cl_2 ^{58–60} and related⁶¹ adducts of Rh are known more generally. The rather long Rh–Cl distance measured is consistent with its orientation *trans* to a strongly σ -donating alkyl ligand.⁶⁰ The formation of solvent adducts, such as $3[\text{BARF}_4]$, by displacement of weakly bound alkane ligands at low temperature is well-established.^{24, 62} While the *anti*-arrangement of Rh1–H and C18–H does not unambiguously define that the same orientation is present in $2[\text{BARF}_4]$ it does offer strong support for such an orientation being present in this alkane complex.

Complex $3[\text{BARF}_4]$ decomposes to a mixture of products at room temperature in CD_2Cl_2 , and so NMR spectroscopic data were collected at 193 K. In the solution $^{31}\text{P}\{^1\text{H}\}$ NMR spectrum two environments are observed, at δ 98.8 [$J(\text{PP})$, 289 Hz; $J(\text{RhP})$ 127 Hz] and at δ –16.5 [$J(\text{PP})$ 289 Hz; $J(\text{RhP})$ 90 Hz]. These data are similar to the SSNMR data for $2[\text{BARF}_4]$, suggesting a closely related structure for the phosphine ligand. In the solution ^1H NMR spectrum a hydride signal is observed at δ –28.43 as a doublet of doublets of doublets, that collapses to a doublet in the $^1\text{H}\{^{31}\text{P}\}$ NMR spectrum [$J(\text{PH}) = 7, 12$ Hz; $J(\text{RhH})$ 64 Hz]. The methine proton on C18 is identified at δ 1.67 by an unusually large coupling to ^{31}P [$J(\text{PH}) = 49$ Hz, 1 H], that collapses in the $^1\text{H}\{^{31}\text{P}\}$ NMR spectrum. Vacuum transfer of the volatiles, dissolving in CD_2Cl_2 and interrogation by ^1H NMR spectroscopy shows the formation of NBA, further supporting the assignment of $2[\text{BARF}_4]$.

Identification of a probable intermediate: $[\text{Rh}(\text{dtbbp})(\text{NBE})][\text{BARF}_4]$, $4[\text{BARF}_4]$. Given the significant structural reorganisation that accompanies the *in crystallo* formation of the NBA complex, $2[\text{BARF}_4]$, the order of events

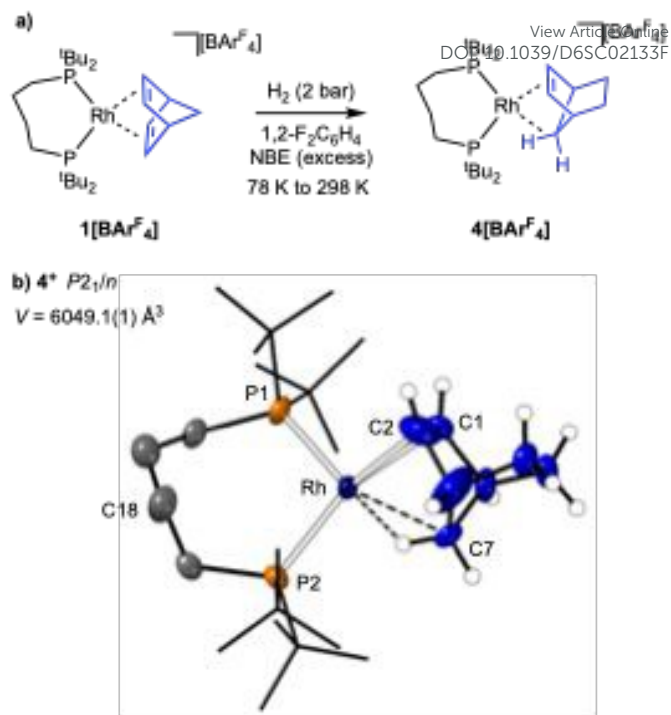


Figure 8 a) Synthesis of $4[\text{BARF}_4]$ b) Solid-state structure of one of the crystallographically-independent cations of 4^+ . Displacement ellipsoids are shown that the 30% probability level, selected H-atoms shown, ^tBu groups shown in stick form. Selected bond distance (Å) and angles ($^\circ$): Rh1–P1, 2.3222(12); Rh1–P2, 2.3678(11); Rh1–C1, 2.262(6); Rh1–C2, 2.225(9); Rh1...C7 2.366(9); P1–Rh1–P2, 102.03(5); P1–Rh1–C7, 155.29(16); P2–Rh1–mid(C1/C2) 154.02(4).

leading to this complex was of interest. In particular, when does C–H activation of the phosphine backbone occur? As the NBD ligand requires to be hydrogenated twice to form NBA, presumably via a norbornene (NBE) intermediate, the independent synthesis of this complex was attempted to see if C–H activation had occurred, Figure 8a.

$[\text{Rh}(\text{dtbbp})(\text{NBE})][\text{BARF}_4]$, $4[\text{BARF}_4]$, was isolated as purple crystalline material, by the solution hydrogenation of excess NBD where H_2 is the limiting reagent using $1[\text{BARF}_4]$ as a catalyst, followed by low temperature recrystallisation (-30 °C). The molecular structure of $4[\text{BARF}_4]$ (Figure 8b) shows an NBE ligand coordinated to a Rh(I) centre by the *exo*-face of the alkene and an agostic $\text{Rh}\cdots\text{H}-\text{C}$ interaction, $\text{Rh}\cdots\text{C7} = 2.366(9)$ Å. The phosphine backbone is not C–H activated, retaining the *cis*- κ^2 -P,P motif of the starting material. As the isolated yield of $4[\text{BARF}_4]$ was poor (15 %), characterisation by SSNMR or onward SC–SC reactivity was not attempted.⁶³ Complex $4[\text{BARF}_4]$ is unstable at room temperature in CD_2Cl_2 , but low temperature solution NMR data for $4[\text{BARF}_4]$ are fully consistent with both the solid-state structure, and previously-reported NBE complexes.^{31, 64} Notably the agostic $\text{Rh}\cdots\text{H}-\text{C}$ group is observed at δ –5.67 as a broad signal in the ^1H NMR spectrum; while in the $^{31}\text{P}\{^1\text{H}\}$ NMR spectrum two environments are observed at δ 90.3 [$J(\text{RhP})$ 220 Hz; $J(\text{PP})$ 19 Hz] and δ 30.0 [$J(\text{RhP})$ 142 Hz; $J(\text{PP})$ 19 Hz]. The arrangement of $[\text{BARF}_4]^-$ anions around the cation is very similar to that observed for $1[\text{BARF}_4]$, $2[\text{BARF}_4]$ and $3[\text{BARF}_4]$



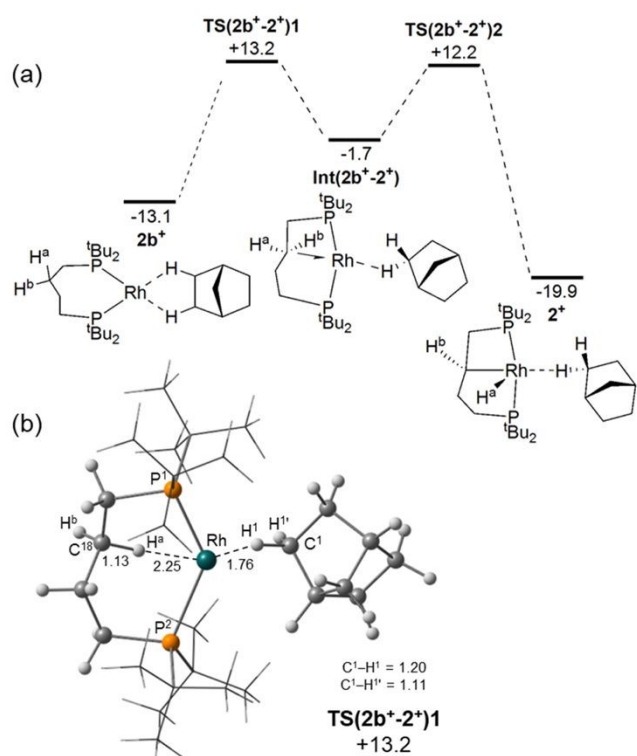
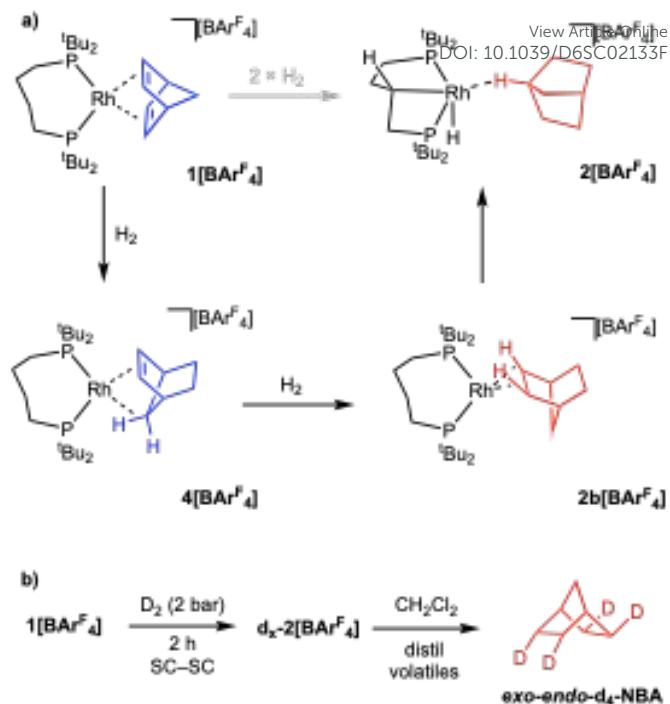


Figure 9. a) Computed reaction profile (free energies, kcal/mol relative to $4^* + \text{H}_2$) for backbone C-H activation in $2b^*$. Level of theory: PBE-D3(def2-tzvp)//PBE-D3(SDD(Rh, P, with d-orbital polarization on P); 6-31g** other atoms). b) Computed structure of $\text{TS}(2b^+-2^*)1$ (selected distances in Å; ^tBu groups in wireframe).

(ESI), with the unit cell volume only 1.6% larger than in the starting complex, $1[\text{BAR}^f_4]$.

To probe the sequence of events that transform $1[\text{BAR}^f_4]$ into $2[\text{BAR}^f_4]$, C-H activation of the phosphine backbone was modelled via DFT calculations on the isolated *cis*- κ^2 -P,P cations $[\text{Rh}(\text{dtbbp})(\text{L}_2)]^+$, where $\text{L}_2 = \text{NBD} (1^+)$, $\text{NBE} (4^+)$ and $\text{NBA} (2b^+)$, a putative $\eta^2\eta^2$ -NBA-bound precursor to C-H activation. The computed thermodynamics indicate backbone C-H activation is significantly endergonic at 1^+ ($\Delta G = +15.3$ kcal/mol), becomes more accessible at 4^+ ($\Delta G = +0.9$ kcal/mol), and is exergonic at $2b^+$ ($\Delta G = -6.8$ kcal/mol). The competition between backbone C-H activation and NBE hydrogenation was therefore computed at 4^+ and showed the latter to proceed with a barrier of 14.8 kcal/mol to give $2b^+$ at -13.1 kcal/mol. In comparison backbone activation in 4^+ is kinetically less accessible ($\Delta G^\ddagger = 18.9$ kcal/mol, see Figure S49). This implies that $4[\text{BAR}^f_4]$ is unlikely to have a significant lifetime in the presence of available H_2 and will instead react to form $2[\text{BAR}^f_4]$ via NBE hydrogenation, followed by backbone C-H activation. In the absence of H_2 , backbone C-H activation in 4^+ is a kinetically accessible, if slightly endergonic (and hence reversible) process.

The computed reaction profile for backbone C-H activation at $2b^+$ (Figure 9a) involves opening the P2-Rh-P3 angle, coupled with rearrangement of the C_4 -backbone to form agostic intermediate $\text{Int}(2b^+-2^*)$ at -1.7 kcal/mol. C-H activation via $\text{TS}(2b^+-2^*)$ at $+12.2$ kcal/mol to form the *anti*-isomer of 2^+ at -19.9 kcal/mol. Both $\text{Int}(2b^+-2^*)$ and 2^+ feature the NBA ligand bound primarily through an *endo* C-H bond.



Scheme 4. a) Proposed order of events in the *in crystallo* formation of $2[\text{BAR}^f_4]$ from H_2 addition to $1[\text{BAR}^f_4]$. b) Formation of *exo-endo*- d_4 -NBA from addition of D_2 to $1[\text{BAR}^f_4]$

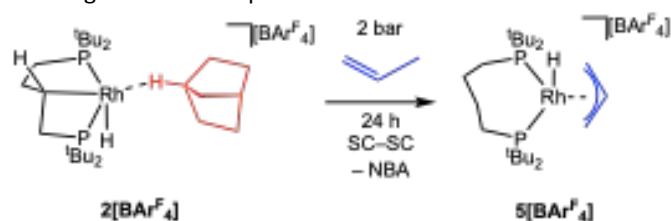
With this isolated cation model the bridgehead C-H bond structure observed in the crystal structure is 1.6 kcal/mol higher in energy. C-H activation therefore has an overall barrier of $+26.3$ kcal/mol with the rate-limiting transition state, $\text{TS}(2b^+-2^*)1$, corresponding to P-Rh-P angle opening and backbone rearrangement (Figure S50).

Scheme 4a shows the overall proposed order of events, which also support the work of Goldman and Krogh-Jespersen on oxidative addition of C-H bonds in d^8 - MXL_2 -type complexes.⁶⁵ Their studies showed that stronger σ -donating ligands *trans* to the site of C-H activation disfavour oxidative addition. In the system here, C-H activation of the ligand backbone is thermodynamically preferred for σ -alkane intermediate $2b[\text{BAR}^f_4]$, rather than the alkene complex $4[\text{BAR}^f_4]$.

Supporting evidence for the intermediate role of $4[\text{BAR}^f_4]$ comes from addition of D_2 to crystalline $1[\text{BAR}^f_4]$ to ultimately form d_4 - $2[\text{BAR}^f_4]$, as confirmed by SSNMR and single-crystal X-ray diffraction, Scheme 4b. Dissolving the resulting crystals in CD_2Cl_2 , vacuum transfer of the volatiles, and analysis by ^2H NMR spectroscopy and GC-MS shows the exclusive formation of *exo-endo*- d_4 -NBA.^{66, 67} This is consistent with initial addition of D_2 to the *endo*-face of NBD in $1[\text{BAR}^f_4]$, a rearrangement to form $4[\text{BAR}^f_4]$, and then addition of the second equivalent of D_2 to the *exo*-face of NBE. We have previously noted both selective *exo-endo*²¹ and *endo-endo*³¹ NBD hydrogenation *in crystallo*, and suggest these differences come from variations in the primary and secondary microenvironment that influence the barrier to rearrangement of NBE.⁶⁸ Addition of D_2 to single crystals of $2[\text{BAR}^f_4]$ resulted in no H/D exchange at the NBA (by GC/MS and ^1H NMR spectroscopy), in contrast with



[Rh(Cy₂P(CH₂)₂PCy₂)(η²-η²-NBA)][BAR^F₄] where selective exchange that the *exo* positions is observed.^{31, 69}



Scheme 5. Synthesis of 5[BAR^F₄].

A structurally responsive ligand and reversible C–H activation:

Addition of propene to [Rh(dtbpb)(NBA)][BAR^F₄]. The calculated differences in the thermodynamics of C–H activation of the phosphine backbone in 1⁺, 2b⁺ and 4⁺ suggested that modification of the ligand *trans* to the position of C–H activation might promote reductive elimination. We thus targeted the synthesis of complexes where the alkane ligand was replaced, in an *in crystallo* substitution. While addition of a variety of gases to single crystals of 2[BAR^F₄] (CO, ethene, butene, 1,3-butadiene) did result in a reaction, there was also loss of crystallinity and the formation of intractable products. However, addition of propene to 2[BAR^F₄] resulted in a clean SC-SC transformation over 24 hr, to give a product of empirical formula [Rh(dtbpb)(C₃H₆)] [BAR^F₄], 5[BAR^F₄], Scheme 5. While the crystals do not change colour, they become coated in an oily-solid, presumably liberated NBA, that could be removed by application of a dynamic vacuum (5 × 10⁻³ mbar) for 18 h.

As shown by a resulting single-crystal X-ray diffraction study at 110 K, Figure 10a, substitution of NBA with propene reverses C–H activation of the phosphine bridge, reforming the κ²-*cis*-P,P ligand motif observed in the NBA and NBE adducts. There is a space group change to C2/c that results in a superposition of two cationic fragments related by a C₂ axis, which sit in the ~O_h cage of [BAR^F₄]⁻ anions, Figure 10b. This complexity is exacerbated by a two-component twin model being needed for a reasonable structural model, R₁ = 9.74%. While the resulting

structural solution unambiguously showed formation of the κ²-*cis*-P,P ligand and NBA had been lost, it did not allow for the discrimination between a propene or an allyl-hydride ligand, as the C–C distances were lightly restrained and crystallographically identical [1.45(5) and 1.46(3) Å].

Vacuum transfer of CD₂Cl₂ onto these single crystals resulted in a temperature sensitive solution of 5[BAR^F₄]. NMR spectra recorded at 193 K showed a single environment in the ³¹P{¹H} NMR spectrum at δ 65.3 [J(RhP) = 131 Hz]; at a chemical shift similar to 1[BAR^F₄], but with a coupling constant to ¹⁰³Rh more like 2[BAR^F₄]. In the ¹H NMR spectrum an upfield-shifted doublet of triplets (1 H) was observed at δ -32.55 [J(RhP) = 40 Hz; J(PH) 12 Hz], that collapses into a doublet on decoupling ³¹P. Three, mutually coupled, resonances are observed at δ 5.09 (1H), 4.82 (2H) and 2.36 (2H). Collectively these data identify the low temperature solution structure as being a Rh(III) allyl-hydride, [Rh(dtbpb)(H)(η³-C₃H₅)] [BAR^F₄]. Warming CD₂Cl₂ solutions of 5[BAR^F₄] to room temperature resulted in decomposition to multiple products. In the solid-state the ³¹P{¹H} SSNMR spectrum recorded at 183 K shows two signals at δ 59 and 73; while in the ¹³C{¹H} SSNMR spectrum two broad environments are observed at δ 63 and 68 in the region associated with alkene or allyl ligands.⁵⁶ Warming to +20 °C results in a small chemical shift change to δ 63 and 70 in the ³¹P{¹H} SSNMR spectrum, Figure 10c. However, the corresponding ¹³C{¹H} SSNMR spectrum at +20 °C is now featureless in the region associated with alkene or allyl groups, δ 110 to 50. These data are all consistent with the chelating phosphine ligand adopting a κ²-motif throughout, as there is no-evidence for *trans*-P,P coupling, as observed for 2[BAR^F₄], that is a reporter for a κ³-ligand binding mode.

These data are also consistent with a rapid, at room temperature, non-degenerate fluxional process occurring in the crystalline solid-state for the allyl ligand. Coupled with the solution-determined low temperature structure of an allyl hydride we propose an equilibrium is established *in crystallo*

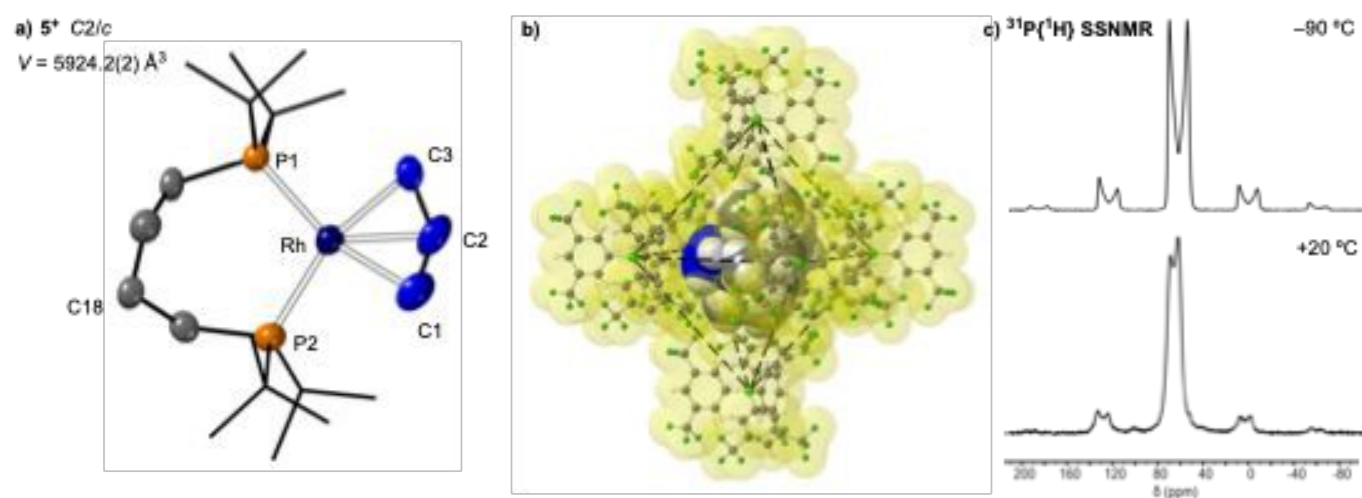


Figure 10 Solid-state structure of one of the disordered components 5[BAR^F₄] a) Structure of the cation, 5⁺. Displacement ellipsoids are shown at the 30% probability level, H-atoms not shown, ^tBu groups shown in stick form. The Rh–hydride was not located. Selected bond lengths (Å) and angles (°). Rh1–P1, 2.363(5); Rh1–P2, 2.327(5); C1–C2, 1.45(5); * C2–C3 1.46(5); * Rh1–C1, 2.21(3); Rh1–C2, 2.18(2); Rh1–C3, 2.21(3); P1–Rh–P2, 105.39(15). * Restrained at 1.47(1) Å. b) Arrangement of [BAR^F₄]⁻ anions around one of the cations. van der Waals radii. c) Variable temperature ³¹P{¹H} SSNMR spectra (162 MHz, 10 kHz spin rate, -90 °C and +20 °C)



between Rh(III) allyl hydride and Rh(I) propene complexes, both of which have a κ^2 -*cis*-P,P ligand motif, that favours the former at low temperature. Fluxional behaviour between propene and allyl/hydride tautomers has been noted before *in crystallo* for [Rh(Cy₂P(CH₂)₂PCy₂)(C₃H₅)] [BAR^F₄].³⁴ In contrast with **5**[BAR^F₄], the Rh(I) propene tautomer for this complex is observed at low temperature, consistent with smaller bite angle phosphine ligands with less bulky groups favouring Rh(I) over Rh(III) oxidation states in such equilibria.⁷⁰ Supporting this finely balanced equilibrium, the previously reported butenes complex [Rh(^tBu₂P(CH₂)₃P^tBu₂)(C₄H₈)] [BAR^F₄]⁴³ exists as an equilibrium mixture of allyl hydride and alkene complexes at 183 K (CD₂Cl₂), in-line with the smaller bite angle associated with the C₃-backbone compared with the C₄ backbone in **5**[BAR^F₄] [cf NBD complexes P–Rh–P 96.75(2)^o versus 102.11(2)^o respectively].

The addition of propene to **2**[BAR^F₄] thus results in a change in the thermodynamics of C–H activation of the phosphine backbone, so that on swapping the very weak σ -donor NBA for propene/allyl hydride C–H activation is now disfavoured, and the structurally responsive phosphine ligand adopts a κ^2 -binding mode in a SC-SC transformation. This observation is also consistent with the initial formation of **2**[BAR^F₄], which occurs from C–H activation at the σ -alkane complex **2b**[BAR^F₄], rather than the NBE precursor, **4**[BAR^F₄].

Conclusions

Ligands that adapt their coordination mode in response to other changes around the metal centre play an important role in organometallic synthesis and catalysis. We demonstrate here that such adaptability is also possible in solid/gas *in crystallo* organometallic reactivity, in which a *cis*-chelating phosphine undergoes reversible C–H activation to form a *trans*-spanning pincer-type ligand in response to the identity of the ligand that sits opposite. Our combined experimental and DFT studies indicate that C–H activation (oxidative addition) occurs at the Rh(I) centre when this ligand is a weakly-binding alkane (NBA) rather than the more strongly binding alkene (NBD), and that when the alkane ligand is exchanged *in crystallo* for an alkene (propene) this C–H activation is reversed to reform the Rh(I) centre. As well as showcasing the power of the *in crystallo* approach for the synthesis, characterisation and stabilisation of σ -alkane complexes, it allows for the reversible adaptivity of the chelating phosphine ligand to be revealed, highlighting how versatile the crystalline solid-state environment can be. Given the wide-spread utilisation of cooperative and responsive ligands in solution homogeneous catalysis this suggests that similar non-innocence is possible *in crystallo*.

Author contributions

The manuscript was written by contributions from all the Authors. JCG led the experimental investigations, corresponding data analysis and writing the first draft. MAS led the computational investigation.

SKF performed initial synthetic investigations. KMA contributed to experimental work and data analysis. TSCH developed enabling code for the computational investigation. GJT and MRW contributed to data collection and analysis on the Diamond I19 beamline. SJP performed solid-state NMR experiments. JML was a co-supervisor of JGC, alongside ASW. ASW and SAM were responsible for writing the final draft, and overall conceptualisation and supervision of the project.

Conflicts of interest

There are no conflicts to declare.

Acknowledgements

The EPSRC (DTP award to JCG; EP/W015552/1, KA; EP/W015498/1, MAS); SCG Chemicals (SKF); ERC (PRECISION SMOM, Project Number 101198896, HORIZON-ERC, ERC-2024-ADG). JML is supported by a Royal Society Industry Fellowship (INF\R1\221057)

Notes and references

- J. R. Khusnutdinova and D. Milstein, Metal–Ligand Cooperation, *Angew. Chem. Int. Ed.*, 2015, *54*, 12236–12273
- L. Alig, M. Fritz and S. Schneider, First-Row Transition Metal (De)Hydrogenation Catalysis Based On Functional Pincer Ligands, *Chem. Rev.*, 2019, *119*, 2681–2751
- M. R. Elsbay and R. T. Baker, Strategies and mechanisms of metal–ligand cooperativity in first-row transition metal complex catalysts, *Chem. Soc. Rev.*, 2020, *49*, 8933–8987
- L. V. A. Hale and N. K. Szymczak, Hydrogen Transfer Catalysis beyond the Primary Coordination Sphere, *ACS Catal.*, 2018, *8*, 6446–6461
- A. Rossin and M. Peruzzini, Ammonia–Borane and Amine–Borane Dehydrogenation Mediated by Complex Metal Hydrides, *Chem. Rev.*, 2016, *116*, 8848–8872
- J. M. Blacquiere, Structurally-Responsive Ligands for High-Performance Catalysts, *ACS Catal.*, 2021, *11*, 5416–5437
- G. M. Adams and A. S. Weller, POP-type ligands: Variable coordination and hemilabile behaviour, *Coord. Chem. Rev.*, 2018, *355*, 150–172
- Y. Guari, G. P. F. van Strijdonck, M. D. K. Boele, J. N. H. Reek, P. C. J. Kamer and P. W. N. M. van Leeuwen, Palladium-Catalyzed Amination of Aryl Bromides and Aryl Triflates Using Diphosphane Ligands: A Kinetic Study, *Chem. Eur. J.*, 2001, *7*, 475–482
- S. Acosta-Calle and A. J. M. Miller, Tunable and Switchable Catalysis Enabled by Cation-Controlled Gating with Crown Ether Ligands, *Acc. Chem. Res.*, 2023, *56*, 971–981
- A. F. Orsino, M. Gutiérrez del Campo, M. Lutz and M.-E. Moret, Enhanced Catalytic Activity of Nickel Complexes of an Adaptive Diphosphine–Benzophenone Ligand in Alkyne Cyclotrimerization, *ACS Catal.*, 2019, *9*, 2458–2481
- H. D. Empsall, E. M. Hyde, R. Markham, W. S. McDonald, M. C. Norton, B. L. Shaw and B. Weeks, Synthesis and X-ray structure of an unusual iridium ylide or carbene complex, *J. Chem. Soc., Chem. Commun.*, 1977, 589–590



- 12 J. M. Brown, P. A. Chaloner, A. G. Kent, B. A. Murrer, P. N. Nicholson, D. Parker and P. J. Sidebottom, The mechanism of asymmetric homogeneous hydrogenation. Solvent complexes and dihydrides from rhodium diphosphine precursors, *J. Organomet. Chem.*, 1981, *216*, 263–276
- 13 C. Crocker, R. J. Errington, W. S. McDonald, K. J. Odell, B. L. Shaw and R. J. Goodfellow, Rapid reversible fission of a C–H bond in a metal complex: X-ray crystal structure of $[\text{RhCl}(\text{Bu}^t_2\text{PCH}_2\text{CH}_2\text{CH}_2\text{CH}_2\text{P}^t\text{Bu}_2)]$, *J. Chem. Soc., Chem. Commun.*, 1979, 498–499
- 14 A. Vignalok, Y. Ben-David and D. Milstein, Complexation of N_2 , H_2 , CO_2 , and Ethylene to a T-Shaped Rhodium(I) Core, *Organometallics*, 1996, *15*, 1839–1844
- 15 J. Zhou and J. F. Hartwig, Iridium-Catalyzed H/D Exchange at Vinyl Groups without Olefin Isomerization, *Angew. Chem. Int. Ed.*, 2008, *47*, 5783–5787
- 16 D. Gelman and S. Musa, Coordination Versatility of sp^3 -Hybridized Pincer Ligands toward Ligand–Metal Cooperative Catalysis, *ACS Catal.*, 2012, *2*, 2456–2466
- 17 K. M. Altus, S. K. Furfari, J. Goodall, M. R. Gyton, J. Heaton, C. Johnson, A. I. McKay, M. Sondrup Møller, S. D. Pike and A. S. Weller, Solid-state Molecular Organometallic Chemistry (SMOM): A Users' Guide to In Crystallo Single-Crystal to Single-Crystal Transformations using Solid/Gas Methods, *Dalton Trans.*, 2026, DOI: 10.1039/D6DT00444J
- 18 K. A. Reid and D. C. Powers, In crystallo organometallic chemistry, *Chem. Commun.*, 2021, *57*, 4993–5003
- 19 A. Sur and D. C. Powers, In Crystallo Photochemistry: Reimagining Synthetic Tractability with Transparent Single-Crystalline Flasks, *ACS Cent. Sci.*, 2025, *11*, 834–842
- 20 S. D. Pike, F. M. Chadwick, N. H. Rees, M. P. Scott, A. S. Weller, T. Krämer and S. A. Macgregor, Solid-State Synthesis and Characterization of σ -Alkane Complexes, $[\text{Rh}(\text{L}_2)(\eta^2, \eta^2\text{-C}_7\text{H}_{12})][\text{BAr}^f_4]$ (L_2 = Bidentate Chelating Phosphine), *J. Am. Chem. Soc.*, 2015, *137*, 820–833
- 21 S. D. Pike, A. L. Thompson, A. G. Algarra, D. C. Apperley, S. A. Macgregor and A. S. Weller, Synthesis and Characterization of a Rhodium(I) σ -Alkane Complex in the Solid State, *Science*, 2012, *337*, 1648–1651
- 22 J. D. Watson, L. D. Field and G. E. Ball, Binding methane to a metal centre, *Nature Chem.*, 2022, *14*, 801–804
- 23 S. Geftakis and G. E. Ball, Direct Observation of a Transition Metal Alkane Complex, $\text{CpRe}(\text{CO})_2(\text{cyclopentane})$, Using NMR Spectroscopy, *J. Am. Chem. Soc.*, 1998, *120*, 9953–9954
- 24 W. H. Bernskoetter, C. K. Schauer, K. I. Goldberg and M. Brookhart, Characterization of a Rhodium(I) σ -Methane Complex in Solution, *Science*, 2009, *326*, 553–556
- 25 P. J. Sempstrott, B. B. Trinh, C. F. Lovitt, N. E. Capra and G. S. Girolami, An osmium(II) methane complex: Elucidation of the methane coordination mode, *Science Adv.*, 2023, *9*, eadg8130
- 26 M. Sellin, J. D. Watson, J. Fischer, G. E. Ball, L. D. Field and I. Krossing, Promoting Alkane Binding: Crystallization of a Cationic Manganese(I)-Pentane σ -Complex from Solution, *Angew. Chem. Int. Ed.*, 2025, *64*, e202507494
- 27 J. C. Mullins, M. J. Evans, J. M. Parr, D. T. Nguyen, A. I. McKay, T. Rajeshkumar, R. O. Piltz, A. J. Edwards, L. Maron and C. Jones, Alkane Coordination by a Neutral, Lewis Acidic Magnesium Complex, *J. Am. Chem. Soc.*, 2025, *147*, 47584–47594
- 28 N. R. Andreychuk and D. J. H. Emslie, Potassium–Alkane Interactions within a Rigid Hydrophobic Pocket, *Angewandte Chemie*, 2013, *125*, 1740–1743
- 29 J. Jung, S. T. Löffler, J. Langmann, F. W. Heinemann, F. Bill, G. Biston, W. Scherer, M. Atanasov, K. Meyer and F. Neese, Dispersion Forces Drive the Formation of Uranium–Alkane Adducts, *J. Am. Chem. Soc.*, 2020, *142*, 1864–1870
- 30 M. A. Bogachev, A. N. Selikhov, A. V. Cherkasov, R. R. Aysin, S. S. Bukalov and A. A. Trifonov, Intermolecular Lithium η^2 -Alkene and κ^2 -Alkane Complexes: Synthesis, Bonding, and Facile Interconversion, *J. Am. Chem. Soc.*, 2025, *147*, 34610–34619
- 31 F. M. Chadwick, T. Krämer, T. Gutmann, N. H. Rees, A. L. Thompson, A. J. Edwards, G. Buntkowsky, S. A. Macgregor and A. S. Weller, Selective C–H Activation at a Molecular Rhodium Sigma-Alkane Complex by Solid/Gas Single-Crystal to Single-Crystal H/D Exchange, *J. Am. Chem. Soc.*, 2016, *138*, 13369–13378
- 32 A. I. McKay, A. J. Bukvic, B. E. Tegner, A. L. Burnage, A. J. Martínez-Martínez, N. H. Rees, S. A. Macgregor and A. S. Weller, Room Temperature Acceptorless Alkane Dehydrogenation from Molecular σ -Alkane Complexes, *J. Am. Chem. Soc.*, 2019, *141*, 11700–11712
- 33 M. R. Gyton, M. A. Sajjad, D. J. Storm, K. M. Altus, J. C. Goodall, C. L. Johnson, S. J. Page, A. J. Edwards, R. O. Piltz, S. B. Duckett, S. A. Macgregor and A. S. Weller, An Operationally Unsaturated Iridium-Pincer Complex That C–H Activates Methane and Ethane in the Crystalline Solid-State, *J. Am. Chem. Soc.*, 2025, *147*, 8706–8719
- 34 F. M. Chadwick, A. I. McKay, A. J. Martínez-Martínez, N. H. Rees, T. Krämer, S. A. Macgregor and A. S. Weller, Solid-state molecular organometallic chemistry. Single-crystal to single-crystal reactivity and catalysis with light hydrocarbon substrates, *Chem. Sci.*, 2017, *8*, 6014–6029
- 35 K. M. Altus, Y. Shi, P. Probst, J. H. Heaton, M. R. Gyton, L. Lari, M. R. Buchmeiser, P. W. Dyer and A. S. Weller, Room Temperature Ethene to Propene (ETP) Tandem Catalysis using Single Crystalline Solid-State Molecular Pre-Catalysts, *Angew. Chem. Int. Ed.*, 2025, *64*, e202419923
- 36 C. L. Johnson, D. J. Storm, M. A. Sajjad, M. R. Gyton, S. B. Duckett, S. A. Macgregor, A. S. Weller, M. Navarro and J. Campos, A Gold(I)–Acetylene Complex Synthesised using Single-Crystal Reactivity, *Angew. Chem. Int. Ed.*, 2024, *63*, e202404264
- 37 J. C. Goodall, M. A. Sajjad, E. A. Thompson, S. J. Page, A. M. Kerrigan, H. T. Jenkins, J. M. Lynam, S. A. Macgregor and A. S. Weller, In crystallo lattice adaptivity triggered by solid-gas reactions of cationic group 7 pincer complexes, *Chem. Commun.*, 2023, *59*, 10749–10752
- 38 C. L. Johnson, K. M. Altus, M. Navarro, J. Campos, S. B. Duckett and A. S. Weller, Single-crystal to single-crystal synthesis of a gold(I)-ammonia complex and H/D exchange in crystallo with D_2O , *Dalton Trans.*, 2025, *54*, 16673–16676
- 39 K. M. Altus, M. A. Sajjad, M. R. Gyton, A. C. Whitwood, S. J. Page, S. A. Macgregor and A. S. Weller, Solid/Gas In Crystallo Reactivity of an Ir(I) Methylidene Complex, *Organometallics*, 2024, *43*, 3137–3142
- 40 L. R. Doyle, M. R. Galpin, S. K. Furfari, B. E. Tegner, A. J. Martínez-Martínez, A. C. Whitwood, S. A. Hicks, G. C. Lloyd-Jones, S. A. Macgregor and A. S. Weller, Inverse Isotope Effects in Single-Crystal to Single-Crystal Reactivity and the Isolation of a Rhodium Cyclooctane σ -Alkane Complex, *Organometallics*, 2022, *41*, 284–292
- 41 A. J. Martínez-Martínez, B. E. Tegner, A. I. McKay, A. J. Bukvic, N. H. Rees, G. J. Tizzard, S. J. Coles, M. R. Warren, S. A. Macgregor and A. S. Weller, Modulation of σ -Alkane Interactions in $[\text{Rh}(\text{L}_2)(\text{alkane})]^+$ Solid-State Molecular Organometallic (SMOM) Systems by Variation of the Chelating Phosphine and Alkane: Access to η^2, η^2 - σ -Alkane Rh(I), η^1 - σ -Alkane Rh(III) Complexes, and Alkane Encapsulation, *J. Am. Chem. Soc.*, 2018, *140*, 14958–14970
- 42 M. A. Sajjad, S. A. Macgregor and A. S. Weller, A comparison of non-covalent interactions in the crystal structures of two σ -alkane



complexes of Rh exhibiting contrasting stabilities in the solid state, *Faraday Diss.*, 2023, **244**, 222–240

43 S. K. Furfari, B. E. Tegner, A. L. Burnage, L. R. Doyle, A. J. Bukvic, S. A. Macgregor and A. S. Weller, Selectivity of Rh...H–C Binding in a σ -Alkane Complex Controlled by the Secondary Microenvironment in the Solid State, *Chem. Eur. J.*, 2021, **27**, 3177–3183

44 A. J. Bukvic, A. L. Burnage, G. J. Tizzard, A. J. Martínez-Martínez, A. I. McKay, N. H. Rees, B. E. Tegner, T. Krämer, H. Fish, M. R. Warren, S. J. Coles, S. A. Macgregor and A. S. Weller, A Series of Crystallographically Characterized Linear and Branched σ -Alkane Complexes of Rhodium: From Propane to 3-Methylpentane, *J. Am. Chem. Soc.*, 2021, **143**, 5106–5120

45 A. L. B. A. G. Algarra, M. Iannuzzi, T. Krämer, S. A. Macgregor, R. E. M. Pirie, B. Tegner and A. S. Weller, ed. D. M. P. M. a. P. R. Raithby, Springer International Publishing, Cham, 2020, pp. 183–228.

46 N. E. Capra, B. B. Trinh and G. S. Girolami, Weakly Bound but Strongly Interacting: The Structures, Stabilities, and Dynamics of Osmium(II) Ethane, Propane, and Butane Complexes, *J. Am. Chem. Soc.*, 2025, **147**, 7377–7390

47 D. Amoroso, M. Haaf, G. P. A. Yap, R. West and D. E. Fogg, A Stable Silylene in a Reactive Environment: Synthesis, Reactivity, and Silicon Extrusion Chemistry of a Coordinatively Unsaturated Ruthenium Silylene Complex Containing Chloride and η^3 -P–C–P Ligands, *Organometallics*, 2002, **21**, 534–540

48 C. S. Durfy, J. A. Zurakowski, G. Jobin and M. W. Drover, An Investigation of Allyl-Substituted Bis(Diphosphine) Iron Complexes: Towards Precursors for Cooperative CO₂ Activation, *Chem. Eur. J.*, 2024, **30**, e202302721

49 A. Das, C.-H. Wang, G. P. Van Trieste, III, C.-J. Sun, Y.-S. Chen, J. H. Reibenspies and D. C. Powers, In Crystallo Snapshots of Rh₂-Catalyzed C–H Amination, *J. Am. Chem. Soc.*, 2020, **142**, 19862–19867

50 Z.-J. Lv, K. A. Eisenlohr, R. Naumann, T. Reuter, H. Verplancke, S. Demeshko, R. Herbst-Irmer, K. Heinze, M. C. Holthausen and S. Schneider, Triplet carbenes with transition-metal substituents, *Nature Chem.*, 2024, **16**, 1788–1793

51 O. V. Ozerov, C. Guo, V. A. Papkov and B. M. Foxman, Facile Oxidative Addition of N–C and N–H Bonds to Monovalent Rhodium and Iridium, *J. Am. Chem. Soc.*, 2004, **126**, 4792–4793

52 A. B. Chaplin, J. C. Green and A. S. Weller, C–C Activation in the Solid State in an Organometallic σ -Complex, *J. Am. Chem. Soc.*, 2011, **133**, 13162–13168

53 I. J. Vitórica-Yrezábal, S. Libri, J. R. Loader, G. Mínguez Espallargas, M. Hippler, A. J. Fletcher, S. P. Thompson, J. E. Warren, D. Musumeci, M. D. Ward and L. Brammer, Coordination Polymer Flexibility Leads to Polymorphism and Enables a Crystalline Solid–Vapour Reaction: A Multi-technique Mechanistic Study, *Chem. Eur. J.*, 2015, **21**, 8799–8811

54 M. K. Panda, S. Ghosh, N. Yasuda, T. Moriwaki, G. D. Mukherjee, C. M. Reddy and P. Naumov, Spatially resolved analysis of short-range structure perturbations in a plastically bent molecular crystal, *Nature Chem.*, 2015, **7**, 65–72

55 I. J. Vitórica-Yrezábal, C. A. McAnally, M. P. Snelgrove, M. R. Warren, A. H. Hill, S. P. Thompson, M. Quinn, S. Mottley, S. Mottley, A. J. Fletcher and L. Brammer, Selective CO₂ uptake mimics dissolution in highly fluorinated non-porous crystalline materials, *Nature Chem.*, 2025, **17**, 1705–1711

56 P. S. Pregosin, *NMR in Organometallic Chemistry*, Wiley-VCH, Weinheim, 2012.

57 P. Pracht, S. Grimme, C. Bannwarth, F. Bohle, S. Ehlert, G. Feldmann, J. Gorges, M. Müller, T. Neudecker, C. Platt, S. Spicher, P. Steinbach, P. A. Wesolowski and F. Zeller, CREST—A program for the exploration of low-energy molecular chemical space, *J. Chem. Phys.*, 2024, **160**, 114110

58 B. K. Corkey, F. L. Taw, R. G. Bergman and M. Brookhart, Aromatic and aldehyde carbon–hydrogen bond activation at cationic Rh(III) centers. Evaluation of electronic substituent effects on aldehyde binding and C–H oxidative addition, *Polyhedron*, 2004, **23**, 2943–2954

59 G. M. Adams, F. M. Chadwick, S. D. Pike and A. S. Weller, A CH₂Cl₂ complex of a [Rh(pincer)]⁺ cation, *Dalton Trans.*, 2015, **44**, 6340–6342

60 R. C. Knighton, J. Emerson-King, J. P. Rourke, C. A. Ohlin and A. B. Chaplin, Solution, Solid-State, and Computational Analysis of Agostic Interactions in a Coherent Set of Low-Coordinate Rhodium(III) and Iridium(III) Complexes, *Chem. Eur. J.*, 2018, **24**, 4927–4938

61 A. Longcake, M. R. Lees, M. S. Senn and A. B. Chaplin, Oxidative Addition of C–Cl Bonds to a Rh(PONOP) Pincer Complex, *Organometallics*, 2022, **41**, 3557–3567

62 M. D. Walter, P. S. White, C. K. Schauer and M. Brookhart, Stability and Dynamic Processes in 16VE Iridium(III) Ethyl Hydride and Rhodium(I) σ -Ethane Complexes: Experimental and Computational Studies, *J. Am. Chem. Soc.*, 2013, **135**, 15933–15947

63 The in crystallo solid/gas addition of D₂ to a precursor NBE complex closely related to **4**[BAR^f₄], gives *exo*-D₂-NBA. See ref [31]

64 Peter H. M. Budzelaar, Nicolle N. P. Moonen, René d. Gelder, Jan M. M. Smits and Anton W. Gal, Rhodium and Iridium β -Diiminate Complexes – Olefin Hydrogenation Step by Step, *Eur. J. Inorg. Chem.*, 2000, 753–769

65 D. Y. Wang, Y. Choliy, M. C. Haibach, J. F. Hartwig, K. Krogh-Jespersen and A. S. Goldman, Assessment of the Electronic Factors Determining the Thermodynamics of “Oxidative Addition” of C–H and N–H Bonds to Ir(I) Complexes, *J. Am. Chem. Soc.*, 2016, **138**, 149–163

66 R. R. Schrock and J. A. Osborn, Catalytic hydrogenation using cationic rhodium complexes. II. The selective hydrogenation of alkynes to *cis* olefins, *J. Am. Chem. Soc.*, 1976, **98**, 2143–2147

67 B. Nguyen and J. M. Brown, Stereoselectivity in the Rhodium-Catalysed Reductions of Non-Conjugated Dienes, *Adv. Syn. Catal.*, 2009, **351**, 1333–1343

68 The observation of d₄-NBA is also consistent with NBE hydrogenation preceding backbone C–H activation; an alternative pathway in which backbone C–H activation in **4**⁺ occurred prior to D₂--addition would lead to the formation of a Rh–D (see Figure S48/49). Moreover, assuming facile formation of **2b**⁺, such a process would be both kinetically ($\Delta G^\ddagger = +31.8$ kcal/mol) and thermodynamically ($\Delta G = +13.8$ kcal/mol) disfavoured compared to backbone C–H activation directly at **2b**⁺ ($\Delta G^\ddagger = +26.3$ kcal/mol; $\Delta G = -6.8$ kcal/mol).

69 T. Krämer, F. M. Chadwick, S. A. Macgregor and A. S. Weller, Solid-State Confinement Effects in Selective *exo*-H/D Exchange in the Rhodium σ -Norbornane Complex [(Cy₂PCH₂CH₂PCy₂)Rh(η^2 : η^2 -C₇H₁₂)] [BAR^f₄], *Helv. Chim. Acta*, 2023, **106**, e202200154

70 A. D. Wilson, A. J. M. Miller, D. L. DuBois, J. A. Labinger and J. E. Bercaw, Thermodynamic Studies of [H₂Rh(diphosphine)₂]⁺ and [HRh(diphosphine)₂(CH₃CN)]²⁺ Complexes in Acetonitrile, *Inorg. Chem.*, 2010, **49**, 3918–3926



Data Availability Statement

View Article Online
DOI: 10.1039/D6SC02133F

The Electronic Supplementary Material (ESI) contains full experimental and characterisation data for the new complexes, including single crystal X-ray crystallographic collection and refinement details. Full details of computational studies, including .xyz geometries.

